DOE DE-FG26-06NT-42684

FINAL REPORT

August 2008

TITLE: **Developing Supersonic Impactor and Aerodynamic Lens for Separation and Handling of Nano-Sized particles**

PI: Goodarz Ahmadi

INSTITUTION: Clarkson University
Potsdam, NY 13699-5700
Tel: (315) 268-2322
Fax: (315) 268-4494
Email: ahmadi@clarkson.edu

GRANT NO.: DE-FC26-06-NT42684

PROJECT DURATION: January 1, 2006 to June 30, 2008

DISCLAIMER

Table of Content

Developing Supersonic Impactor and Aerodynamic Lens for Separation and Handling of Nano-Sized particles

Abstract

A computational model for supersonic flows of compressible gases in an aerodynamic lens with several lenses and in a supersonic/hypersonic impactor was developed. Airflow conditions in the aerodynamic lens were analyzed and contour plots for variation of Mach number, velocity magnitude and pressure field in the lens were evaluated. The nano and micro-particle trajectories in the lens and their focusing and transmission efficiencies were evaluated. The computational model was then applied to design of a aerodynamic lens that could generate focus particle beams while operating under atmospheric conditions.

The computational model was also applied to airflow condition in the supersonic/hypersonic impactor. Variations of airflow condition and particle trajectories in the impactor were evaluated. The simulation results could provide understanding of the performance of the supersonic and hypersonic impactors that would be helpful for the design of such systems.

DOE DE-FG26-06NT-42684
FINAL REPORT
August 2008
Cost Status Report

Baseline Reporting Quarter	YEAR 1				YEAR 2				YEAR	
	Q1	Q2	Q3	Q4	Q1	Q2	Q3	Q4	Q1	Q2
Baseline Cost Plan (from SF-424A)	(From 424A, Sect. D)									
Federal Share	$12,500	$12,500	$12,500	$12,500	-0-	-0-	-0-	-0-	-0-	-0-
Non-Federal Share	$2,520	$2,520	$2,520	$2,520	-0-	-0-	-0-	-0-	-0-	-0-
Total Planned (Federal and Non-Federal)	$15,020	$15,020	$15,020	$15,020	-0-	-0-	-0-	-0-	-0-	-0-
Cumulative Baseline Cost	$15,020	$30,040	$45,060	$60,080	$60,080	$60,080	$60,080	$60,080	$60,080	$60,080
Actual Incurred Costs										
Federal Share	$1,974	$1,316	$6,983	-0-	-0-	-0-	$5,136	$8,626	$7,242	$18,723
Non-Federal Share	-0-	-0-	-0-	-0-	-0-	-0-	$14,235	-0-	-0-	$14,235
Total Incurred Costs-Quarterly (Federal and Non-Federal)	$1,974	$1,316	$6,983	-0-	-0-	-0-	$19,371	$8,626	$7,242	$32,958
Cumulative Incurred Costs	$1,974	$3,290	$10,274	$10,274	$10,274	$10,274	$29,645	$38,271	$45,513	$78,470
Variance										
Federal Share	$10,526	$11,184	$5,517	$12,500	-0-	-0-	-5,136	-8,626	-7,242	-18,723
Non-Federal Share	$ 2,520	$2,520	$2,520	$2,520	-0-	-0-	-14,235	-0-	-0-	-14,235
Total Variance-Quarterly (Federal and Non-Federal)	$13,046	$13,704	$8,037	$15,020	-0-	-0-	-19,371	-8,626	-7,242	-32,958
Cumulative Variance	$13,046	$26,750	$34,786	$49,806	$49,806	$49,806	$30,435	$21,809	$14,567	-18,390

TITLE: Developing Supersonic Impactor and Aerodynamic Lens for Separation and Handling of Nano-Sized particles

PI: Goodarz Ahmadi

INSTITUTION: Clarkson University
Potsdam, NY 13699-5700
Tel: (315) 268-2322
Fax: (315) 268-4494
Email: ahmadi@clarkson.edu

GRANT NO.: DE-FG26-06NT42684

PROJECT DURATION: January 1, 2006 to June 30, 2008

DOE Project Officer: Robie Lewis

OBJECTIVES

The general objective of this project is to provide the needed fundamental understanding of supersonic/hypersonic impactors as well as aerodynamic lenses for nano-particle separation and focusing. The specific objectives are:

The specific objectives are:

- To develop a design for supersonic/hypersonic impactor for nano-particle separation.
- Develop a design for aerodynamic lenses for generating focused beams of nano-particles.
- Perform a series of computational fluid dynamic (CFD) simulations of supersonic/hypersonic impactor and aerodynamic lenses for performance analysis and design optimization.
- Develop a scientific knowledge basis for supersonic/hypersonic impactors and for aerodynamic lenses.

ACCOMPLISHMENTS

A computational model for supersonic flows of compressible gases in an aerodynamic lens with several lenses and in a supersonic/hypersonic impactor was developed. Airflow conditions in the aerodynamic lens were analyzed and contour plots for variation of Mach number, velocity magnitude and pressure field in the lens were evaluated. The nano and micro-particle trajectories in the lens and their focusing and transmission efficiencies were evaluated. The computational model was also applied to airflow condition in the supersonic/hypersonic impactor. Variations of airflow condition and particle trajectories in the impactor were evaluated.

SIGNIFICANCE TO FOSSIL ENERGY PROGRAM

Developing effective supersonic/hypersonic impactors for nano-particle separation is of considerable interest for production of efficient catalysts for co-production of synthetic fuel and electric power in connection the FutureGen clean coal energy initiative. Also developing aerodynamic lenses for generating focused beams of nano-particles are critical to characterization of these materials.

Final Report

AERODYNAMIC LENS SYSTEM WITH ORIFICES

Variations of airflow condition including Mach number, pressure and velocity contours in the aerodynamic lens system were simulated. The particle trajectory analysis was discussed and the effect of Brownian motion was studied. Sample particle trajectories were also reported. The performance of the aerodynamic lens system was also discussed.

Formulation

In this section, the governing equations for the flow modeling and particle tracking are discussed. Along with these, the definitions for the performance characteristics used in this study are stated.

Flow Simulation Model

In the present work, various configurations for the aerodynamic lens were considered and their performances for particle focusing were studies. For the aerodynamic lens systems with axisymmetric nozzles, the axisymmetric version of the compressible Navier-Stokes equation was solved. The flow in the lens is generally laminar as the Reynolds numbers are relatively small.

Governing Equations

Continuity

$$\frac{\partial \rho}{\partial t} + \frac{\partial}{\partial x}\left(\rho v_a\right) + \frac{\partial}{\partial r}\left(\rho v_r\right) + \frac{\rho v_r}{r} = 0 \qquad (1)$$

Axial Momentum

$$\frac{\partial}{\partial t}(\rho v_a)+\frac{1}{r}\frac{\partial}{\partial x}\left(r\rho v_a^{\,2}\right)+\frac{1}{r}\frac{\partial}{\partial r}\left(r\rho v_r v_a\right)=-\frac{\partial p}{\partial x}+\frac{1}{r}\frac{\partial}{\partial x}\left[r\mu\left(2\frac{\partial v_a}{\partial x}-\frac{2}{3}(\nabla\cdot\mathbf{V})\right)\right]+\frac{1}{r}\frac{\partial}{\partial r}\left[r\mu\left(\frac{\partial v_a}{\partial r}+\frac{\partial v_r}{\partial x}\right)\right] \quad (2)$$

Radial Momentum

$$\frac{\partial}{\partial t}(\rho v_r)+\frac{1}{r}\frac{\partial}{\partial x}\left(r\rho v_a v_r\right)+\frac{1}{r}\frac{\partial}{\partial r}\left(r\rho v_r v_r\right)=-\frac{\partial p}{\partial r}+\frac{1}{r}\frac{\partial}{\partial x}\left[r\mu\left(2\frac{\partial v_r}{\partial x}+\frac{\partial v_a}{\partial r}\right)\right]+\frac{1}{r}\frac{\partial}{\partial r}\left[r\mu\left(2\frac{\partial v_r}{\partial r}-\frac{2}{3}(\nabla\cdot\mathbf{V})\right)\right]-2\mu\frac{v_r}{r^2}+\frac{2}{3}\frac{\mu}{r}(\nabla\cdot\mathbf{V})$$

(3)

Energy

$$\rho C_p\left[\frac{\partial T}{\partial t}+\frac{\partial}{\partial x}(v_r T)+\frac{1}{r}\frac{\partial}{\partial r}(r v_a T)\right]=-\frac{Dp}{Dt}+k\nabla^2 T+\Phi \quad (4)$$

Here,

$$\nabla\cdot\mathbf{V}=\frac{\partial v_a}{\partial x}+\frac{\partial v_r}{\partial r}+\frac{v_r}{r} \quad (5)$$

$$\Phi=\mu\left[2\left\{\left(\frac{\partial v_r}{\partial r}\right)^2+\left(\frac{v_r}{r}\right)^2+\left(\frac{\partial v_a}{\partial x}\right)^2\right\}+\left\{\left(\frac{\partial v_a}{\partial r}\right)+\left(\frac{\partial v_r}{\partial x}\right)\right\}^2\right] \quad (6)$$

Note that the viscous stress for compressible fluid is given as

$$\tau=\mu\left[\left(\nabla V+\nabla V^T\right)-\frac{2}{3}(\nabla\cdot V)I\right] \quad (7)$$

Where $\boldsymbol{\tau}$ is stress tensor and $\mathbf{V}$ is the velocity vector.

Particle Equation of Motion

For a dilute gas-particle flow in an aerodynamic lens, a one-way interaction model is used. This means that it is assumed that the particles are carried by the gas flow and the particle phase if too dilute to affect the flow. In this case, the gas flow field can first be evaluated and then be used for evaluation of particle trajectories. Equation of particle motion in a Lagrangian reference frame is given as

$$\frac{dV_i^p}{dt}=\frac{V_i-V_i^p}{\tau}+F_i^L+n_i(t), \quad (8)$$

where V_p is the particle velocity vector, V is the airflow field velocity vector and τ is the particle relaxation time given as,

$$\tau = \frac{\rho_p d_p^2 C_c}{18\mu}. \tag{9}$$

Here ρ_p is the particle density and d_p is the particle diameter, μ is the gas viscosity, and C_c is the Cunningham correction factor for slip correction for drag force estimated using Stokes law. For small particle diameters comparable to the mean free path of the gas, the no-slip condition assumed for deriving stokes law is no longer valid. In order to correct for this assumption, Cunningham correction factor is used. The Cunningham correction factor is given by

$$C_c = 1 + \frac{2\lambda}{d_p}\left[1.257 + 0.4\exp\left(-1.1\left(d_p / 2\lambda\right)\right)\right] \tag{10}$$

In this equation, λ is the mean free path of the gas in microns.

$$\lambda = \frac{23.1T}{P} \tag{11}$$

In the above equation, T and P are the local temperature and pressure in the gas flow field.

The first term on the right hand side of Equation (8) is the Stokes drag force. The second term, $\mathbf{F}^L$, is the Saffman lift force per unit mass and is given by

$$F_i^L = \frac{2Kv^{1/2}d_{ij}}{SD_p(d_{lk}d_{kl})^{1/4}}(V_j - V_j^p) \tag{12}$$

Here, K=2.594 is the coefficient of Saffman's lift force and d_{ij} is the deformation tensor defined as

$$d_{ij} = \frac{1}{2}\left(\frac{\partial V_i}{\partial x_j} + \frac{\partial V_j}{\partial x_i}\right). \tag{13}$$

The expression for the Saffman (1965) lift force given by Equation (12) is a generalization to a three dimensional shear field. Saffman lift force becomes important for high shear flows for particles that are not too small.

The third term on the right hand side of the particle tracking equation is the Brownian force per unit mass, which is very important for submicron particles. The Brownian force is modeled as a Gaussian white noise random process as described by Li and Ahmadi

(1993). Accordingly, at every time step, a random Brownian force given as

$$n_i(t) = G_i \sqrt{\frac{\pi S_o}{\Delta t}} \tag{14}$$

is exerted on the particle. Here, G_i is selected from a population of zero mean unit variance Gaussian random numbers. In Equation (14), S_o is the power spectrum of the Brownian excitation given by

$$S_o = \frac{216 \nu k T}{\pi \rho d_p S^2 C_c} \tag{15}$$

where $k = 1.38 \times 10^{-23}$ J/K is the Boltzmann constant.

Definitions

In order to evaluate and compare the performance of different aerodynamic lens systems, several performance measures are defined. These are, "focusing efficiency," "transmission efficiency," and "Collection index."

Focusing Efficiency

Focusing efficiency is defined as the ratio of the inlet diameter of the aerodynamic lens minus the particle beam diameter at the exit to the inlet diameter. Thus, the focusing ratio varies in the range of 0 to 1, with numerical values close to 1 indicating a high level of focusing.

Transmission Efficiency

A fraction of particles that are introduced at the inlet may deposit on the solid surfaces in the aerodynamic lens due to impaction, interception and/or Brownian diffusion. The transmission efficiency is defined as the percentage of the particles that reach the outlet section.

Collection Index

Collection index is defined as the number of particles passing through a given cross-section area at the exit of the lens system in unit time for unit sampled particle number concentration at the inlet.

Schematics of a Four-Stage Aerodynamic Lens

Orifices are used by various investigators for particle focusing (Liu et al 1995a,b; Zhang et al., 2002; Zhang et al., 2004; Goo, 2002). The schematic of a typical lens system with orifices is shown in the Figure 1. This orifice lens system consists of four stages with the orifice diameters of 6mm, 4mm, 2mm and 1mm. Each stage is separated from the next by a 10 mm long intermediate chamber. The inlet of this system is 12 mm in diameter.

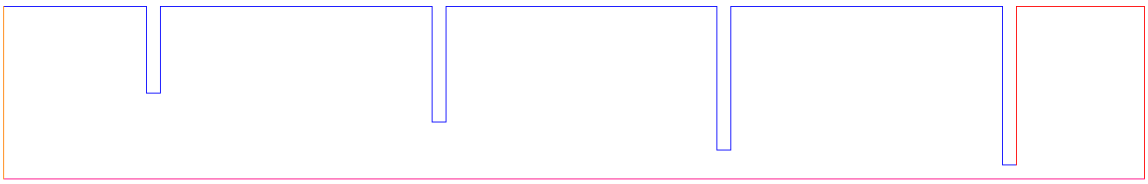

Figure 1. Schematic of a four-stage aerodynamic lens system with orifice.

Computational Model and Grid

The axisymmetric compressible airflow conditions in the converging-diverging nozzle section are evaluated using the Navier-Stokes equation along with the continuity and the energy equations as described by Equations (1)-(7). For the particle beam, the Lagrangian trajectory analysis is used. One-way coupling is assumed in which the particles are carried by the airflow but the effect of particle on the gas flow is neglect. As was noted before, this assumption is reasonable for a dilute particle beam.

For evaluating the flow field in the aerodynamic lens and its downstream chamber, a segregated solver with Reynolds stress transport model was used. This was done using the commercial CFD software FLUENT^{TM} 6.1.22. A rectangular mesh for the computational domain was generated using Gambit^{TM} 2.1.6 software. A uniform grid density of 10/mm was used for the computations. The corresponding grid is shown in Figure 2.

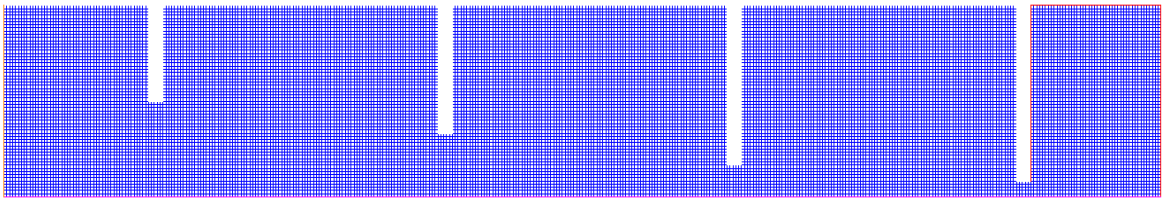

Figure 2 Computation grid of the four-stage aerodynamic lens system with orifices.

Results

In this section, performance of the aerodynamic lenses with orifices in connection with particle focusing is studied. For an atmospheric outlet pressure condition, a series of simulations was performed for different inlet conditions. For various inlet-to-outlet pressure ratios in the range of 2 to 6, the focusing efficiencies of the aerodynamic lens were evaluated. Due to the large variation of pressures, the Cunningham correction factor varies significantly and the assumption of a constant C_c is not correct. The Cunningham correction factor needs to be correctly evaluated at each point. Thus, a Users' Defined Subroutine (UDS) was provided to the discrete phase calculations of the Fluent software. The UDS evaluates the value of the correct Cunningham correction factor at every nodal point based on the values of local temperature and pressure as given by Equations (10) and (11).

Gas Flow Conditions in the Aerodynamic Lens

To provide a better understanding of the focusing and transmission characteristics

of the aerodynamic lens system using the orifices, a series of simulations were performed for given outlet conditions for various pressure ratios. In these cases, the flow field is evaluated considering the pressure outlet condition after the final expansion chamber. In these computations the outlet pressure is considered to be atmospheric and the inlet pressures are obtained form the pressure ratios.

Figure 3 shows the Mach number variations for the aerodynamic lens system. It is observed that the maximum Mach number varies from a value of 1 at a pressure ratio of 2 to a value of 2 for the pressure ratio of 6. The maximum Mach number occurs at the throat of the final stage. The atmospheric exit boundary condition was used here.

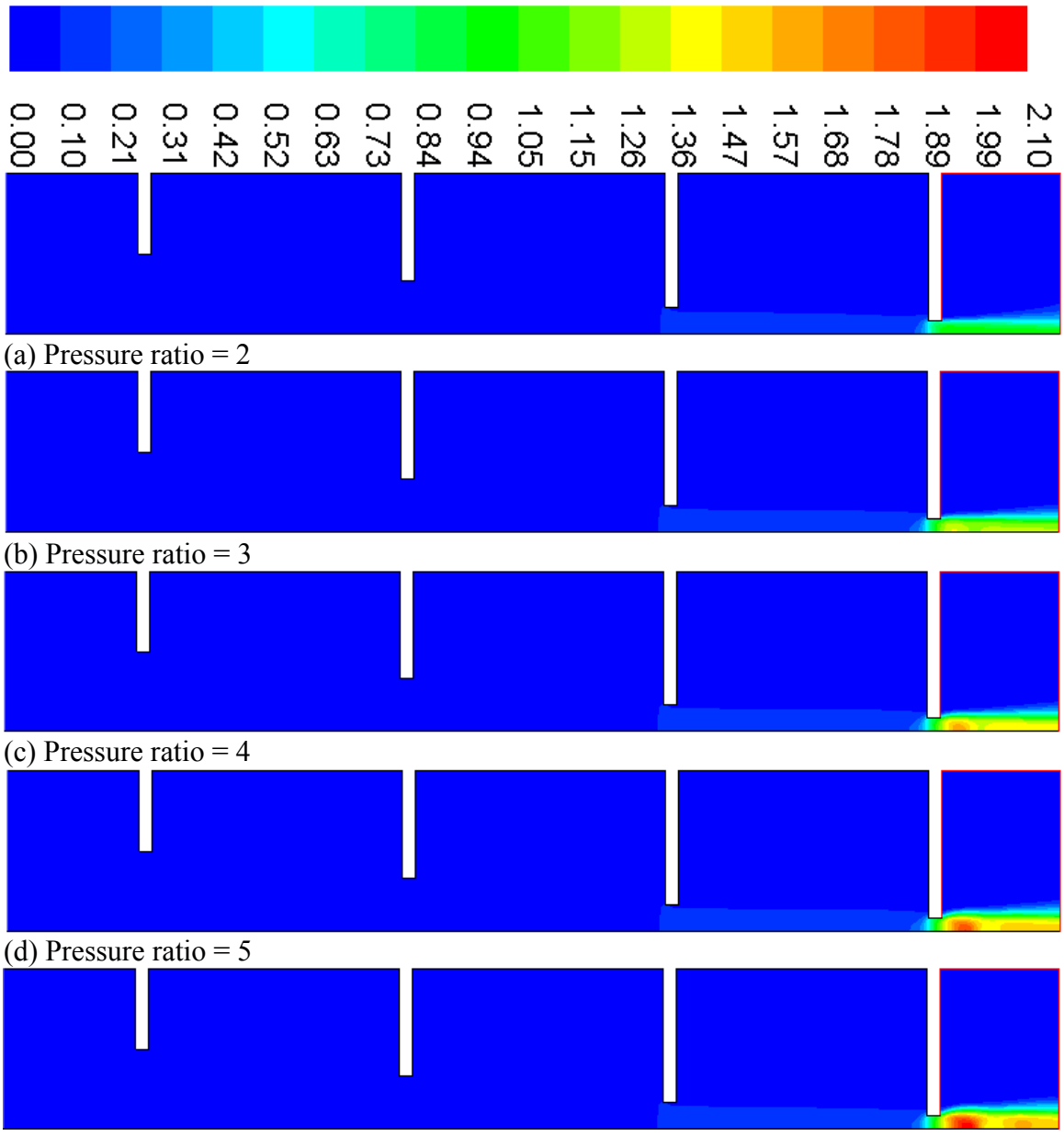

(a) Pressure ratio = 2

(b) Pressure ratio = 3

(c) Pressure ratio = 4

(d) Pressure ratio = 5

(e) Pressure ratio = 6

Figure 3 Mach contours in the aerodynamic system for different pressure ratios.

Figure 4 shows the variations of the velocity contours in the aerodynamic lens system for different pressure ratios. The pressure at the exit was kept fixed at the atmospheric level. It is observed that the velocity increases with the increase of pressure ratio. The peak velocity occurs at the last orifice with smallest diameter. The corresponding streamlines (not shown here due to space limitation) shows that recirculation regions are formed in the intermediate chambers after orifices.

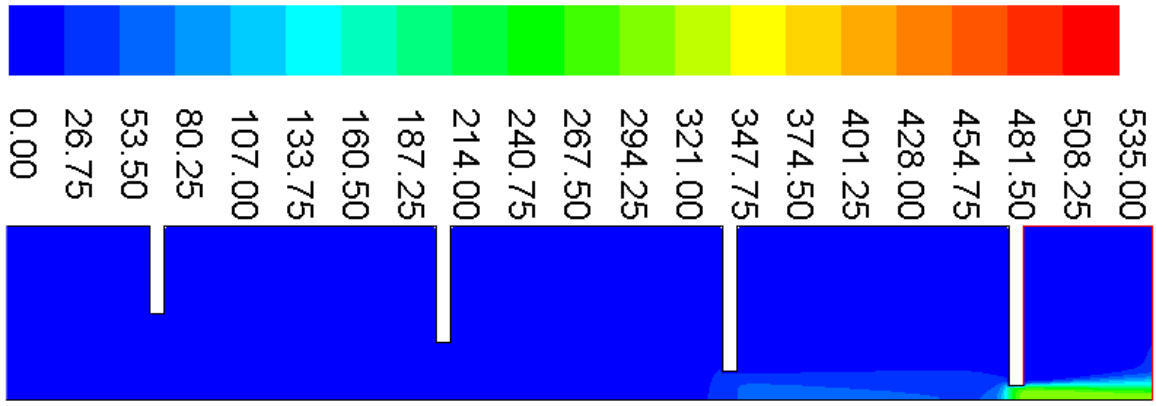

(a) Pressure ratio = 2

(b) Pressure ratio = 3

(c) Pressure ratio = 4

(d) Pressure ratio = 5

(e) Pressure ratio = 6

Figure 4. Velocity magnitude contours in the aerodynamic system with orifices for different pressure ratios with atmospheric outlet pressure.

Figure 5 shows the pressure contour in the aerodynamic lens system for different operating conditions. It is observed that the pressure drop over the first three stages is small and most of the pressure drop occurs at the final stage of the lens system.

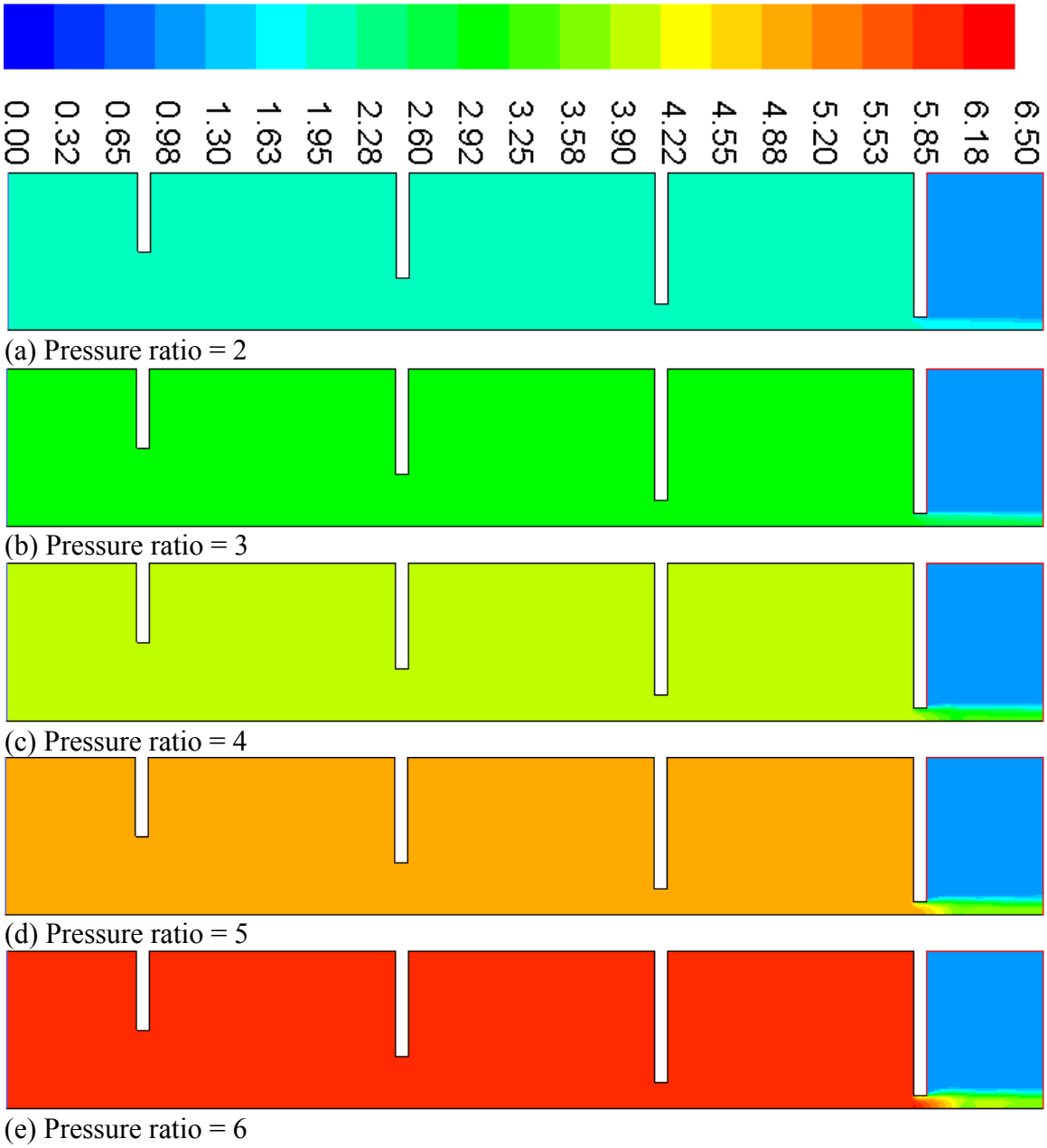

(a) Pressure ratio = 2

(b) Pressure ratio = 3

(c) Pressure ratio = 4

(d) Pressure ratio = 5

(e) Pressure ratio = 6

Figure 5 Pressure contours in the aerodynamic system with orifices for different pressure ratios with atmospheric outlet pressure.

Particle Tracking

In their earlier works, Liu et al (1995a, b) and Zhang et al (2002) considered the orifice geometry for construction of the aerodynamic lens systems. In their works, the Brownian forces were not included on the particles. In both the cases the operating pressures of the less were in the order of few hundred Pascal. Here in the present study,

the operating pressures are atmospheric and important effects of the Brownian diffusion on the particle motion which is very important, especially for nano-particles are included in the analysis. In this section, the effect of Brownian forces on the particle focusing as well as particle transmission efficiencies are studied.

Effect of Brownian Forces on Transmission and Focusing Efficiencies

In order to study the effect of Brownian excitation on transmission efficiency, several simulations were performed. Particular attention was given to the case where the outlet pressure was atmospheric and the pressure ratio was 5. The particle tracking simulations were performed with and without Brownian effects. The results for the transmission efficiencies are listed in the Table 1 and plotted in Figure 6. For the case without Brownian excitation, almost all the particles smaller than 10 micrometer are transmitted through the aerodynamic lens system. However, a large fraction of particles larger than 10 μm are captured. For the case with Brownian excitation Table 1 and Figure 6 show that almost all 1 nm particles are captured. The transmission efficiency then increases with particle diameter up to 10 μm and then decreases with further increase in size.

Table 1 Effect of Brownian excitation on transmission efficiency.

Particle diameter (μm)	With Brownian Excitation	Without Brownian Excitation
0.001	13.90	95.45
0.005	89.55	94.85
0.01	95.85	95.10
0.05	96.05	95.85
0.1	94.41	94.25
0.5	98.95	99.05
1	99.31	99.20
5	99.35	99.30
10	99.24	99.24
50	59.42	59.33
100	56.91	57.05

Table 1 and Figure 6 show that the Brownian effects are more significant for smaller particles. That is, Brownian excitation dominates the dispersion of particles smaller than 50nm. For the particles larger than 50nm, the effects of the Brownian forces are small. For sizes above 1μm, the particle trajectories are not affected by the Brownian forces.

The simulated particle focusing efficiencies are listed in Table 2 and are plotted in Figure 7. The effects of Brownian excitation on focusing efficiency can be seen from this table and figure. The smaller particles appear to not focus well even in the absence of Brownian motion. The smaller particles follow the flow faithfully. Hence these small particles adjust to the sharp changes in the flow direction more readily than the larger particles. This trend is much worsened by the addition of the Brownian excitation that will further broaden the particle beam. Hence the focusing efficiencies without the

Brownian excitation are higher than those with Brownian excitation. As the particle size increases, the Brownian effects decrease and hence the difference between the focusing efficiencies is narrowed down.

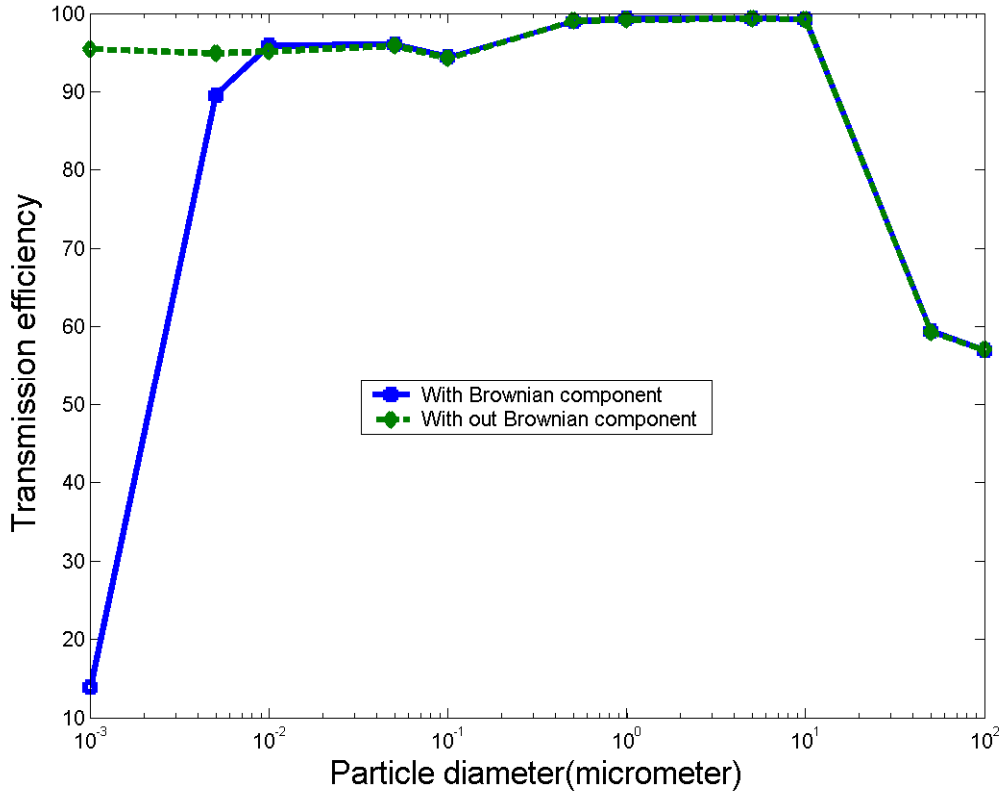

Figure 6. Effect of Brownian forces on Transmission efficiency in orifices.

Table 2. Effect of Brownian excitation on focusing efficiency.

Particle diameter (µm)	With Brownian Excitation	Without Brownian Excitation
0.001	84.53	91.43
0.005	90.47	91.07
0.01	90.92	90.98
0.05	91.10	91.11
0.1	91.35	91.35
0.5	93.46	93.46
1	96.71	96.70
5	96.34	96.33
10	99.07	99.06
50	95.80	95.22
100	93.65	93.65

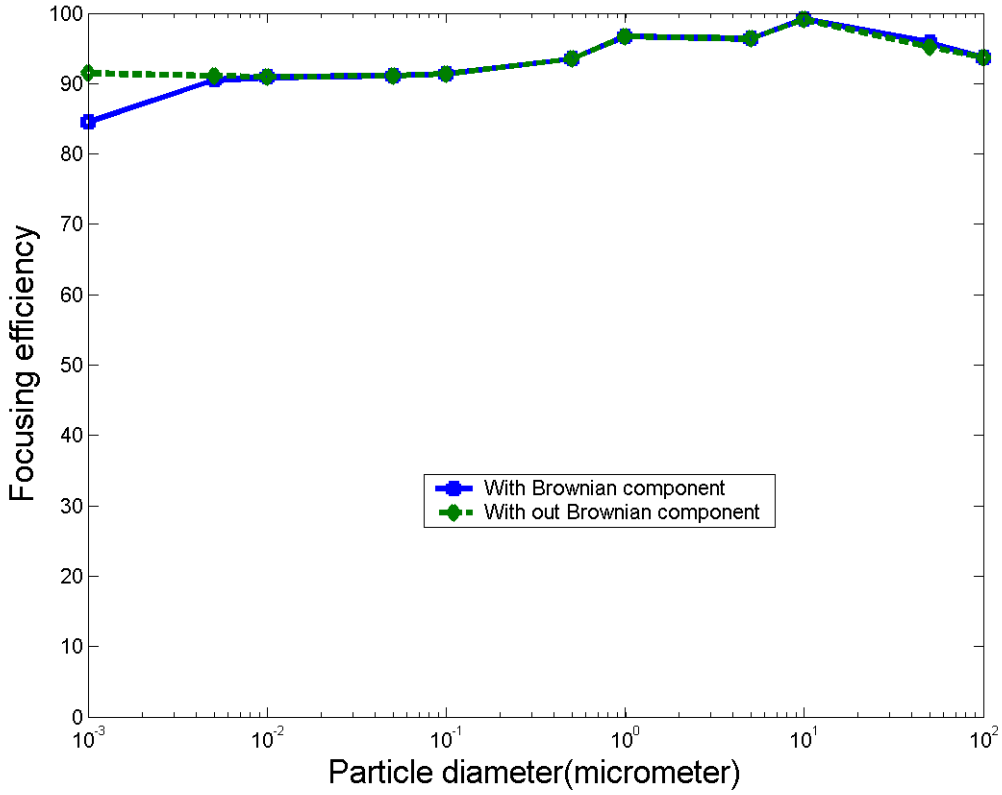

Figure 7. Effect of Brownian forces on focusing efficiency in orifices.

Performance of Five-Stage Aerodynamic Lens

In this section, the simulated particle transmission and focusing efficiencies for the five-stage aerodynamics lens are presented. The lens outlet pressure was kept fixed at 1 atm and pressure ratios from 2 to 6 are considered. In figure 8, sample trajectories for various particle sizes for a pressure ratio of 5 and outlet pressure of 1 atm are shown.

The streamlines are also plotted along with the particle tracks in Figure 8l. Comparison of particle paths with these stream lines shows how the different size particles interact with the flow. The computational results for the five-stage aerodynamic lens system with orifice are listed in the Tables 3 and 4. In Table 3, the transmission efficiencies obtained from the computations for various pressure ratios are tabulated. In Table 4, the simulated focusing efficiencies for various pressure ratios are tabulated. Figures 9 and 10, respectively, show the graphical representation of transmission and focusing efficiencies. It is observed that for the particle size ranges from 10 nm to 10 μm, the transmission efficiencies of more than 80% are obtained using for all the given pressure ratios.

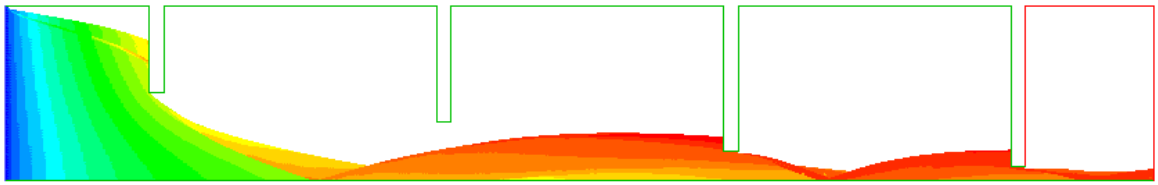

(a) Tracks of 100 µm particles

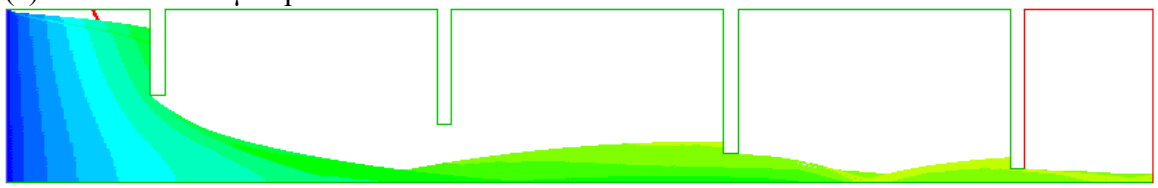

(b) Tracks of 50 µm particles

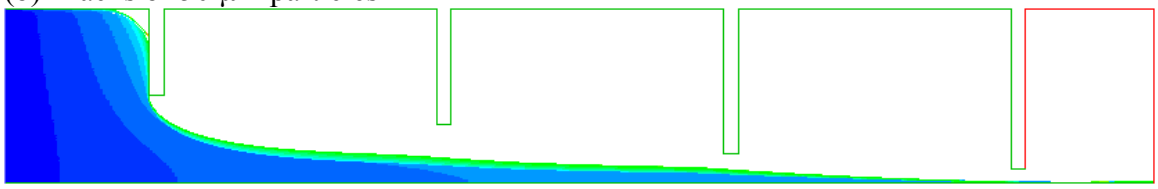

(c) Tracks of 10 µm particles

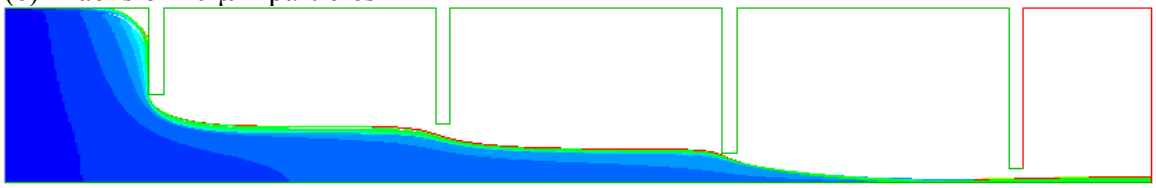

(d) Tracks of 5 µm particles

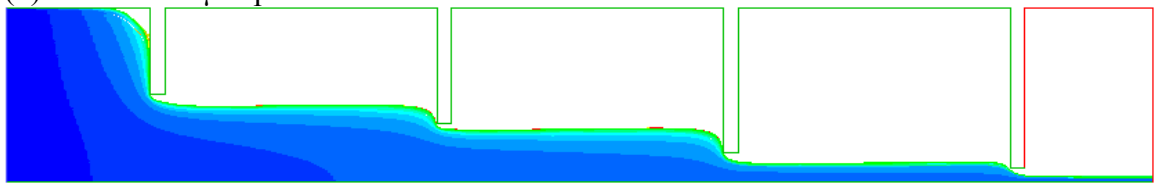

(e) Tracks of 1 µm particles

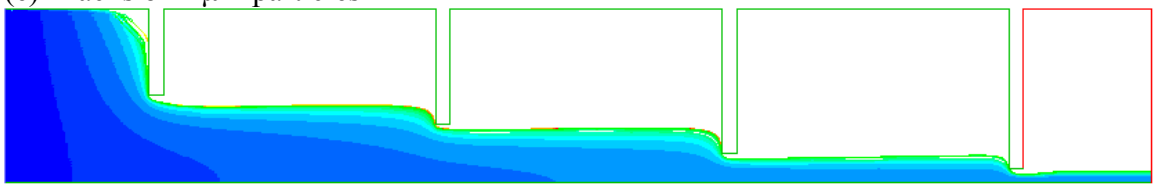

(f) Tracks of 500 nm particles

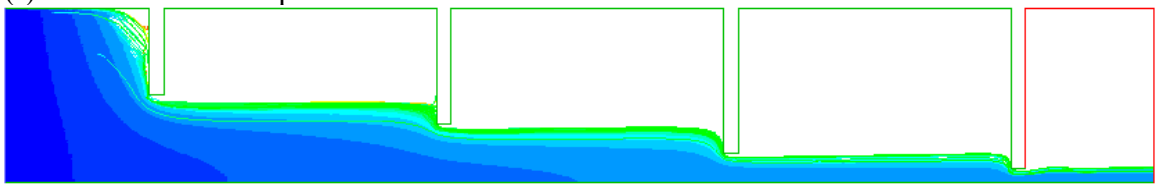

(g) Tracks of 100 nm particles

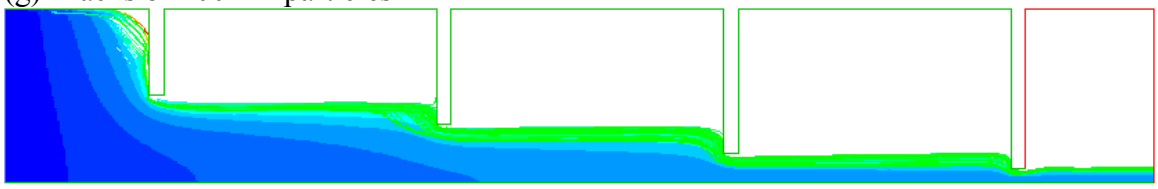

(h) Tracks of 50 nm particles

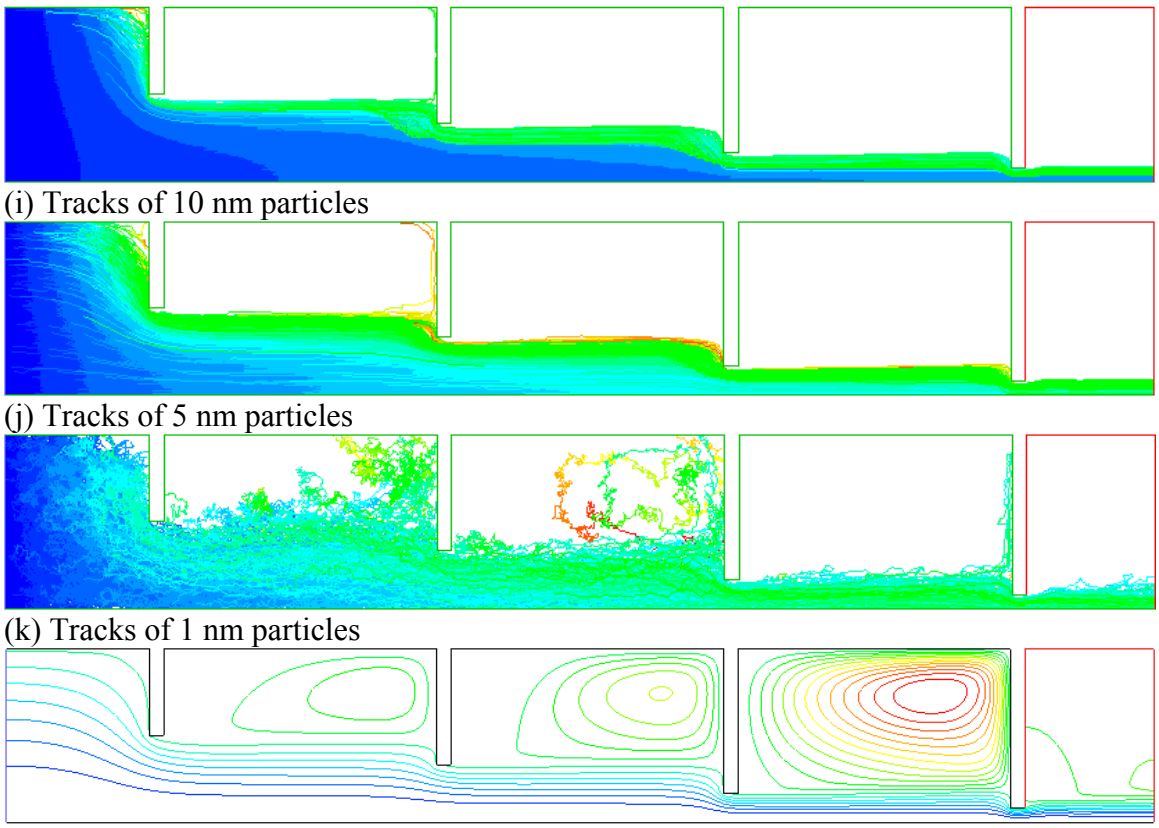

(i) Tracks of 10 nm particles

(j) Tracks of 5 nm particles

(k) Tracks of 1 nm particles

(l) Streamlines for pressure ratio =5

Figure 8. Particle tracks in five-stage aerodynamic lens with orifices.

As noted before, it can be seen that a high fraction of the ultrafine particles are deposited on the walls of the aerodynamic lens. This loss in the transmission efficiency is due to the Brownian diffusion of the small particles. The Brownian excitation dominates the motion of particles smaller than 10nm. As particle size increases, the effect of Brownian excitation decreases. For particle larger than 10 μm, the inertial forces become very high. The inertia effect overwhelms the Brownian effects and also the particle does not respond swiftly to the changes in the flow direction. Thus, the large particles do not follow the flow streamline and are deposited on to the wall of the aerodynamic lens.

Table 3. Transmission efficiencies for various pressure ratios in lens system with orifice.

Particle size (μm)	**Transmission efficiency for outlet pressure 1.0 atm at pressure ratios**				
	2.0	**3.0**	**4.0**	**5.0**	**6.0**
0.001	0.65	4.35	8.45	15.2	18.75
0.005	59.15	77	85.2	89.95	90.85
0.01	87.9	95.15	95.6	95.9	94.85
0.05	93	95.8	96.05	96.2	95.4
0.1	93.95	92.85	94.45	94.45	94.05
0.5	98.25	97.75	98.8	99	98.75
1	99.1	99.6	99.85	99.25	98.8
5	98.85	99.75	99.55	99.4	98.9
10	96.4	98.25	98.9	99.25	99.35
50	67.45	59.4	59.35	59.35	59.5
100	65.55	55	55.8	56.85	59.45

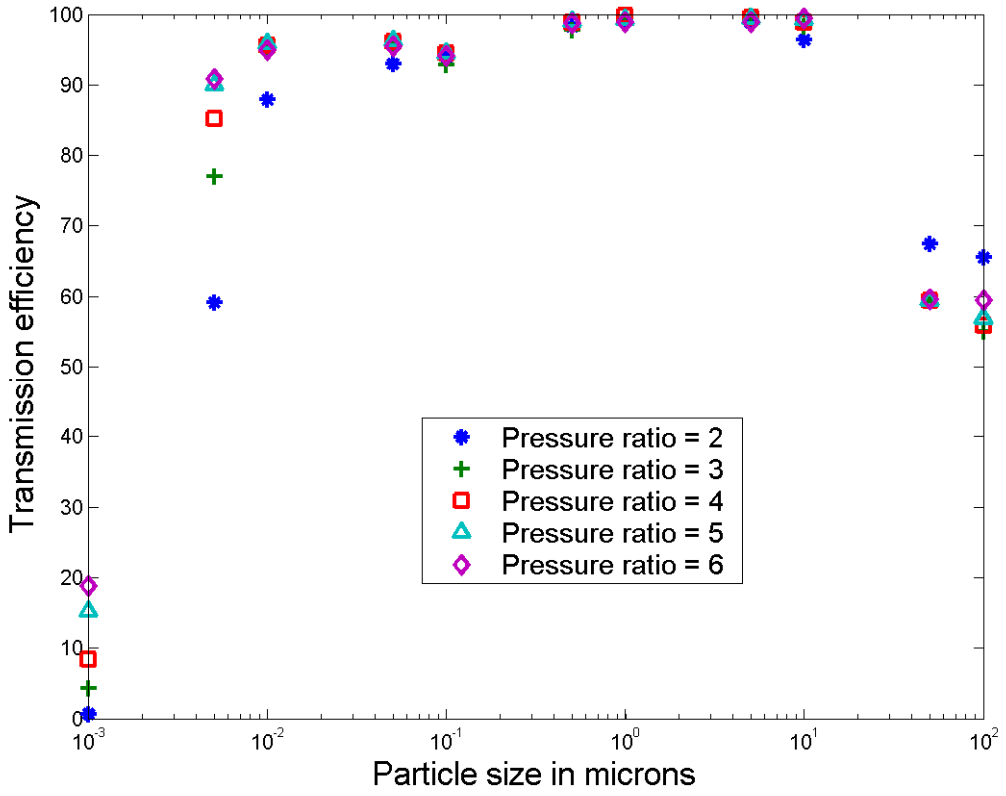

Figure 9. Variation of transmission efficiency with particle size for various pressure ratios in a 5 stage aerodynamic lens system with orifices.

Table 4 Focusing efficiencies for various pressure ratios in lens system with orifice.

Particle size	**Focusing efficiency for outlet pressure 1.0 atm at pressure ratios**				
(μm)	**2.0**	**3.0**	**4.0**	**5.0**	**6.0**
0.001	88.27	81.66	82.18	84.53	80.00
0.005	91.66	90.99	91.48	90.46	90.27
0.01	92.01	91.75	91.25	90.92	90.57
0.05	92.26	92.18	91.72	91.10	90.66
0.1	92.28	92.28	91.89	91.35	90.90
0.5	95.98	95.21	94.30	93.46	92.73
1	98.75	97.94	97.32	96.70	96.30
5	99.57	97.69	96.93	96.34	96.49
10	96.04	98.93	99.04	99.06	99.05
50	84.26	93.33	94.22	93.65	94.57
100	68.33	71.66	70.00	75.80	74.70

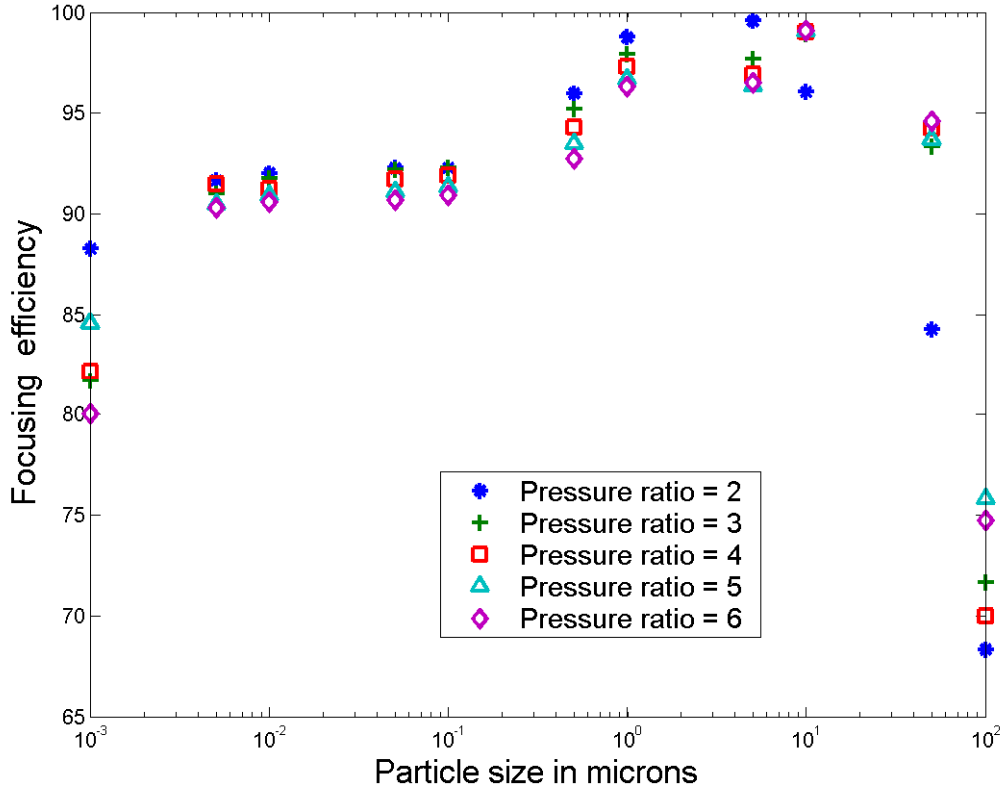

Figure 10. Variation of focusing efficiency with particle size for various pressure ratios in a five-stage aerodynamic lens system with orifices.

Table 5. Stokes numbers based on diameter of the last orifice for a pressure ratio of 5.

Particle diameter in (μm)	**Stokes number**
0.001	1.43e-7
0.005	7.26e-7
0.01	1.47e-6
0.05	8.17e-6
0.1	1.87e-5
0.5	2.1e-4
1	7.41e-4
5	1.63e-2
10	6.43e-2
50	1.58
100	6.33

As for the focusing efficiency, the ultra fine particles are carried by the flow and dispersed by the Brownian motion, thus are not focused properly. With increase in the size of the particles, they get more focused. Particle relaxation time as given by Equation (9) increases with the particle size. Hence in this size range, the particles can not adjust to the very sharp gradients in the flow but can adjust to the more gradual gradients. In the downstream of an orifice, there is a sudden expansion into the intermediate chamber. In this region, the flow changes direction sharply, and particles that are brought to the center line leave the flow streamline and stay focused near the lens centerline. Hence particles with appropriate relaxation time are transported closer and closer to the axis with each stage and hence are focused better.

With further increase in size, the particle inertia becomes so large that they can not even adjust to the gradual changes in the flow as their relaxation times are very larger. Hence, these particles follow their own course and are poorly focused. It is also observed that with an increase in the pressure ratio the transmission efficiencies are improved while the focusing efficiencies are deteriorated.

Conclusions

- Transmission efficiency in the range of 85-99.5% can be obtained for the particles in the size range of 10 nm-10 μm.
- Focusing efficiencies in the range of 90-99% can be obtained for 10 nm-10μm particles.
- Using the five-stage lens, particles smaller than 10 nm can not be focused at atmospheric pressure because of Brownian motion.
- Particles larger than 10 μm have very high transmission losses and are not efficiently focused.

SUPERSONIC/HYPERSONIC IMPACTOR

Model Description

The schematics of an axisymmetric supersonic impactor including upstream nozzle is shown in Figure 11. Flow enters the computational domains with a total pressure P_o and a stagnation temperature T_o. The supersonic impactors are characterized by the L/D ratios. Here L is the distance between the tip of the nozzle and the collection plate, and D is the diameter of the inlet nozzle as shown in Figure 11. It should be noted that the nozzle is a thin plate orifice.

In the simulations, the impactor collection plate and the nozzle walls are treated as solid wall boundaries. At the outlet a constant pressure boundary condition is used. In this study, a fixed nozzle diameter of 0.27 mm is assumed. Nozzle wall sizes are scaled from the one suggested by Fernandez de la Mora et al. (1990). The distance between the nozzle and plate is varied from 0.27 to 5.4 mm. Grid sensitivity study was performed by sequentially refining the computational mesh to reach a solution that was independent of the further refinement of the grid. Finer meshes were used in region with high gradients such as near the bow shock downstream of the nozzle and near the impactor walls.

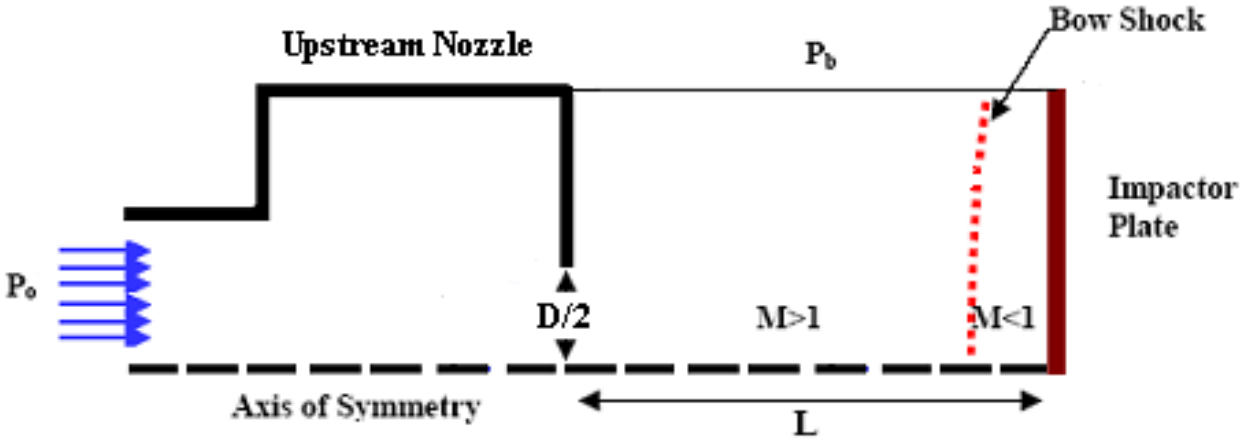

Figure 11. Schematic of the supersonic/hypersonic impactor.

Numerical Method

Figure 12 shows stagnation (total) pressure contours for the case of L/D ratio equal to 3. As noted before, here a pressure ratio of $P_o/P_b = 400$ is assumed. When a supersonic free jet impinges onto a plate, a strong bow shock appears in front of the plate as is shown in the schematics of Figure 11. Figure 12 clearly shows the location and the shape of the bow shock near the impactor plate. Across the bow shock, the stagnation pressure decreases sharply. The computations were done for different L/D ratio and the results show that, as the distance between the nozzle and the impactor plate increases, the

shock becomes stronger.

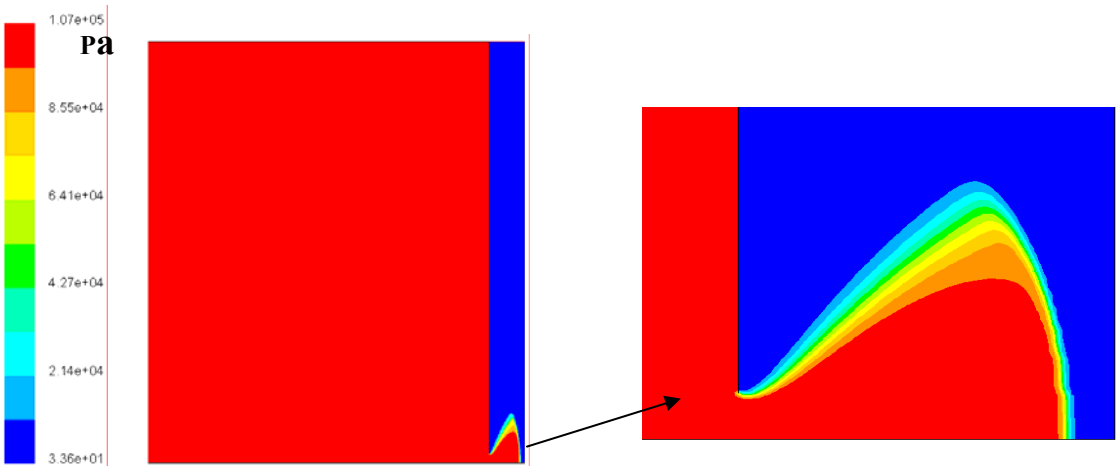

Figure 12. Total pressure contours in the supersonic impactor with L/D = 3 for a pressure ratio of 400.

Performance Analysis

The performance of the supersonic impactor under a range of operating conditions was investigated. Total pressure contours for different L/D ratios are shown in Figure 13. Here a pressure ratio of P_o/P_b = 400 is assumed. When a supersonic free jet impinges onto a plate, a strong bow shock appears in front of the plate. In order to clearly show the structure of the bow shock, most of the upstream nozzle regions are omitted from Figure 13. The location and the shape of the bow shock (called Mach disc) near the impactor plate for different L/D ratios are clearly seen from Figure 13 by the sudden change in total pressure. As the distance between the nozzle and the impactor plate increases, the shock becomes stronger. The distance between the bow shock and impactor plate also increases somewhat with increasing L/D.

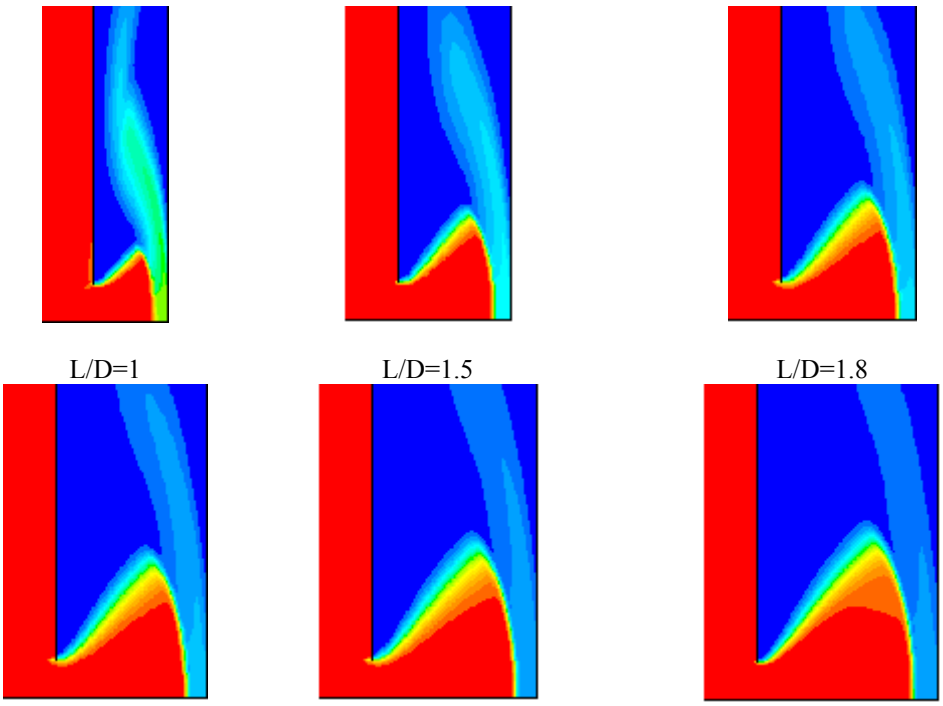

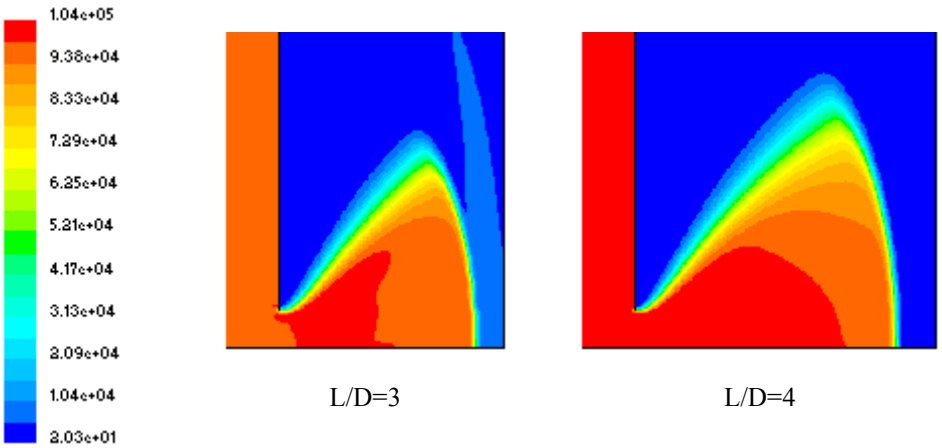

Figure 13. Total pressure contours in the supersonic/hypersonic impactor with different L/D ratios for a pressure ratio of 400.

PUBLICATIONS AND PRESENTATIONS

Journals Articles (peer reviewed)

Abouali, O. and Ahmadi, G., A Model for Supersonic and Hypersonic Impactor, J. Nanoparticle Research, Vol. 7, pp. 75-94 (2005).

Conference Presentations

R.S. Chavali, and G. Ahmadi, "Particle Focusing At Atmospheric Pressures," 24th Annual Conference of the American Association for Aerosol Research, AAAR 2005, Austin, TX, October 17-21, 2005.

R.S. Chavali, G. Ahmadi, and S. Dhaniyala, "Particle Focusing Using Aerodynamic Lens with Slits," 24th Annual Conference of the American Association for Aerosol Research, AAAR 2005, Austin, TX, October 17-21, 2005.

G. Ahmadi, "Supersonic Impactor and Aerodynamic Lens for Nanoparticle Separation," Center for Advanced Material Processing (CAMP) Symposium on Materials Synthesis and Processing, Albany, NY, April 7, 2006.

G. Ahmadi, "Supersonic Impactor and Aerodynamic Lens for Nanoparticle Separation and Computational Modeling Capabilities for Material Processing," Annual Technical Meeting of the Center for Advanced Material Processing (CAMP), Canandaigua, NY, May 17-19, 2006.

A. Zare, O. Abouali and G. Ahmadi, "A Numerical Model for Brownian Motions of Nano-Particles in Supersonic and Hypersonic Impactors," FEDSM2006-98308, ASME 2nd Joint U.S. - European Fluids Engineering Summer Meeting, Miami, FL, July 17-20, 2006.

A. Nikbakht, O. Abouali and G. Ahmadi, **"**3-D Modeling of Brownian Motion of Nano-Particles In Aerodynamic Lenses," FEDSM2006-98488, ASME 2nd Joint U.S. - European Fluids Engineering Summer Meeting, Miami, FL, July 17-20, 2006.

G. Ahmadi, "Applications to Supersonic and Hypersonic Impactors and Aerodynamic Lenses," in Production, Transport and Application of Nanoparticles Workshop/Lecture Series, von Karman Institute for Fluid Dynamics, Brussels, Belgium, February 26 - March 1, 2007.

MILESTONE PLAN/STATUS REPORT

Task/ Subtask #	Critical Path Project Milestone Description*	Project Duration - Start: 01/01/06 End: 12/31/06	Planned Start Date	Planned End Date	Actual Start Date	Actual End Date	Comments
		Project Year (PY) 1					
		Q 1 Q 2 Q 3 Q 4					
Task I	Develop a design for an effective supersonic/ hypersonic impactor for nano-particle separation.		Jan 1 2006	Sept 1 2006	March 2006	June 2008	Lens study was started earlier than the impactor
Task II	Develop a design for aerodynamic lenses for effective generation of narrow focused beams of nano-particles		Jan 1 2006	Oct 1 2006	March 2006	March 2008	Lens study was started earlier than the schedule
Task III	CFD analysis of supersonic/hypersonic impactors		March 1 2006	Nov 1 2006	June 2006	June 2008	Impactor simulation was delayed
Task IV	CFD analysis of aerodynamic lenses		June 1 2006	Dec 31 2006	May 2006	March 2008	Lens simulation was started earlier